Received: 15 July 2019 | Revised: 10 August 2019 | Accepted: 15 August 2019

DOI: 10.37917/ijeee.15.2.1 | Vol. 15 | Issue 2 | December 2019

Open Access

Iraqi Journal for Electrical and Electronic Engineering

Original Article

Bifurcations and Chaos in Current-Driven Induction Motor

Fatma N. Ayoob
Electrical Engineering Department, Basrah University, Basrah, Iraq.
fatmanoori86@gmail.com

Fadhil R. Tahir
Electrical Engineering Department, Basrah University, Basrah, Iraq.
fadhilrahma@hotmail.com

Khalid M. Abdul-Hassan
Electrical Engineering Department, Basrah University, Basrah, Iraq.
Khmh7447@gmail.com

Abstract: *In this paper, a model of PI-speed control current-driven induction motor based on indirect field oriented control (IFOC) is addressed. To assess the complex dynamics of a system, different dynamical properties, such as stability of equilibrium points, bifurcation diagrams, Lyapunov exponents spectrum, and phase portraits are characterized. It is found that the induction motor model exhibits chaotic behaviors when its parameters fall into a certain region. Small variations of PI parameters and load torque affect the dynamics and stability of this electric machine. A chaotic attractor has been observed and the speed of the motor oscillates chaotically. Numerical simulation results are validating the theoretical analysis.*

Index Terms— Indirect Field-Oriented Control (IFOC), Induction Motor, Bifurcation, Chaos.

I. INTRODUCTION

Chaos, also called complex dynamics, is recently one of the most current topics in nonlinear dynamical systems studies [1]. The nonlinear interactions of a system give rise to chaos. Also, it is very sensitive to the system parameters and initial conditions of states. Small variations of these parameters result in great changes in system dynamics [2]. Nowadays, the engineers and industries have paid a lot of attention to the results of specific researches of real systems. Bifurcation is a subfield in nonlinear dynamical systems topics and represents a quantitative measure. The observation of bifurcation diagrams enables one to make a qualitative and quantitative deduction about the behavior and dynamics of the systems. Many theoretical and numerical types of research have been carried out for several qualitative problems in such topics. Practically, the analysis of bifurcation has been applied as a helpful method for exploring the behavior of such systems. They exhibit varieties of bifurcation and chaotic oscillations subjected to period-doubling bifurcation route to chaos [3-5].

Indirect filed oriented controlled (IFOC) induction motor is mostly utilized in industries due to its high torque operation. The parameters of the induction motor may alter with temperature, senility, variation error because of the weakness in valuation algorithms, and other circumferential reasons [6-13]. The IFOC induction motor dynamics is extremely susceptible to differences in the motor configuration; rotor resistance, mutual inductance, stator resistance, inertia, PI controller parameters, and load torque. The performance of a steady-state may have violated due to these variations. Also, the dynamic of the induction motor drive system and may lead to bifurcation in the motor dynamics and consequence; speed and currents fluctuations, variations, or even standing the damage of the motor [14,15]. A quantitative bifurcation can be used for obtaining: 1) the

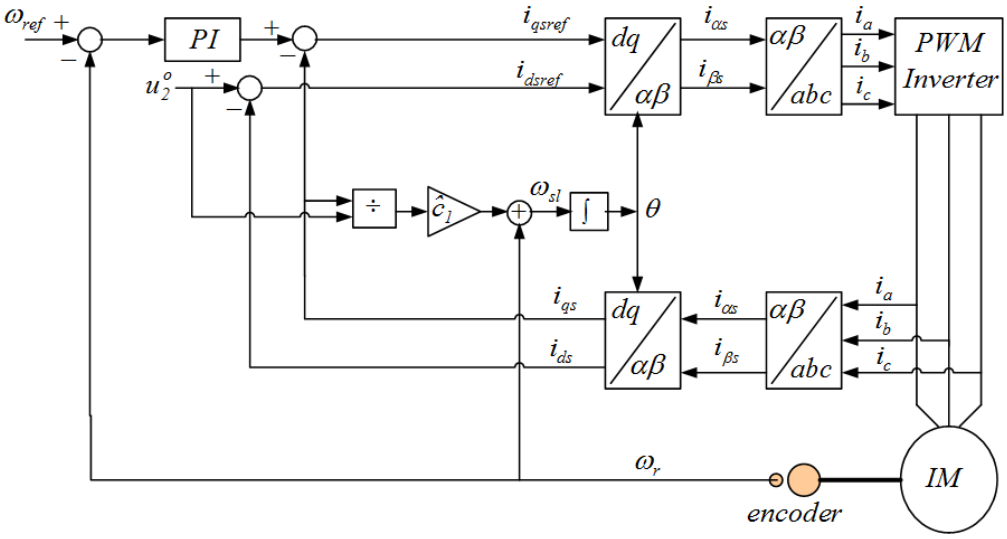

Fig. 1: Speed control scheme of induction motor drive with IFOC system.

stability and robustness; 2) the limiting control gains; 3) the limiting variations in rotor time constant; 4) dangerous bifurcations for avoidance, and 5) the design of efficient controllers for different applications [16-18].

The main objective of this brief will be the bifurcation exploring in the reduced model of current fed induction motor. It is carried out due to the effect of alteration in the PI controller gains and load torque. Bifurcation values of parameters are obtained based on the linearization of the system model near the stationary point. The equilibrium point locus with load torque is also presented. Lyapunov exponents spectrum will be included to confirm the chaotic behavior. The following observations are got from the analysis: 1) the stationary point locus depends on the load torque and rotor resistance estimation; 2) the necessary and sufficient conditions for uniqueness of stationary point; 3) Hopf bifurcation is notable for a specific range of load torque; 4) the avoidance of period-doubling bifurcation can be achieved for higher proportional and lower integral control parameters in the speed feedback. The remnant of this paper is arranged as follows: In Section II, the induction motor adopting IFOC with current fed will be modelled. Based on this model, the stationary points and stability boundaries are discussed. Section III will include the bifurcation diagrams obtained by the numerical simulations due to the effect of PI parameters and load torque. Finally, Section VI draws the paper conclusions.

II. IFOC INDUCTION MOTOR MODEL

A general IFOC on the current-fed induction motor system for speed regulation is shown in Fig.1. The control scheme has a PI controller for speed regulation. The controller output is utilized to produce the torque reference component. The model of IFOC current-driven induction motor can be characterized by [14]

$$\frac{d\psi_{qr}}{dt} = -\frac{R_r}{L_r}\psi_{qr} - \omega_{sl}\psi_{dr} + L_m\frac{R_r}{L_r}i_{qs} \quad (1)$$

$$\frac{d\psi_{dr}}{dt} = -\frac{R_r}{L_r}\psi_{dr} + \omega_{sl}\psi_{qr} + L_m\frac{R_r}{L_r}i_{ds} \quad (2)$$

$$\frac{d\omega_r}{dt} = \frac{3p}{4}\frac{L_m}{L_r J}\left(i_{qs}\psi_{dr} - i_{ds}\psi_{qr}\right) - \frac{B}{J}\omega_r - \frac{T_L}{J} \quad (3)$$

where the subscripts d and q represent the corresponding the direct-axis and quadrature-axis quantities, respectively; ψ_{qr} and ψ_{dr} are the components of the rotor flux; ω_r is the mechanical rotor speed; ω_{sl} is the slip speed, and R_r/L_r is the inverse of rotor time constant. The system parameters are identified in Table 1.

Table 1 System parameters notation

Notation	Description	Notation	Description
R_r	Rotor resistance	B	Friction coeff.
L_m	Mutual inductance	J	Inertia
p	Number of poles	T_L	Load torque
L_r	Rotor inductance	ω_{ref}	Reference speed

The state variables of IFOC induction motor are defined as $x_1 = \psi_{qr}$, $x_2 = \psi_{dr}$, $x_3 = (\omega_{ref} - \omega_r)$, $x_4 = \left(k_p + k_i \int dt\right)(\omega_{ref} - \omega_r)$. Following Fig.1, (1), (2), and (3), the model of IFOC current-driven induction motor can be given as:

$$\dot{x}_1 = -c_1 x_1 + c_2 x_4 - \frac{kc_1}{u_2^0} x_2 x_4 \quad (4)$$

$$\dot{x}_2 = -c_1 x_2 + c_2 u_2^0 + \frac{kc_1}{u_2^0} x_1 x_4 \quad (5)$$

$$\dot{x}_3 = -c_3 x_3 - c_4 \left[c_5 (x_2 x_4 - u_2^0 x_1) - T_L - \frac{c_3}{c_4} \omega_{ref} \right] \quad (6)$$

$$\dot{x}_4 = (k_i - k_p c_3) x_3 - k_p c_4 \left[c_5 (x_2 x_4 - u_2^0 x_1) - T_L - \frac{c_3}{c_4} \omega_{ref} \right] \quad (7)$$

where
$c_1 = \frac{R_r}{L_r}$, $c_2 = \frac{L_m}{L_m} R_r$, $c_3 = \frac{B}{J}$, $c_4 = \frac{1}{J}$, $c_5 = \frac{3p}{4} \frac{L_m}{L_r}$, k_p, and k_i are the speed PI controller gains, $k = \hat{c}_1 / c_1$ is the measure between estimated and real rotor time constant. In general, the IFOC induction motor is fully fluxed by exciting it with a constant $i_{ds} = u_2^0$ while the torque is regulated by controlling i_{qs}.

III. Equilibria and Bifurcations

A. Equilibria

It is essential to characterize the locus, uniqueness, and stability of the equilibrium points of the system (4) - (7) and their dependence on the load torque. The equilibrium point can be deduced by the solutions $\mathbf{x}^e = [x_1^e \; x_2^e \; x_3^e \; x_4^e]^T$ of the system equations:

$$-c_1 x_1^e + c_2 x_4^e - \frac{kc_1}{u_2^0} x_2^e x_4^e = 0 \quad (8)$$

$$-c_1 x_2^e + c_2 u_2^0 + \frac{kc_1}{u_2^0} x_1^e x_4^e = 0 \quad (9)$$

$$-c_3 x_3^e - c_4 \left[c_5 (x_2^e x_4^e - u_2^0 x_1^e) - T_L - \frac{c_3}{c_4} \omega_{ref} \right] = 0 \quad (10)$$

$$(k_i - k_p c_3) x_3^e - k_p c_4 \left[c_5 (x_2^e x_4^e - u_2^0 x_1^e) - T_L - \frac{c_3}{c_4} \omega_{ref} \right] = 0 \quad (11)$$

The fluxes equilibrium values can be obtained from (8) and (9) as

$$x_1^e = \frac{c_2}{c_1} u_2^0 \frac{1-k}{1+k^2 z^2} z \quad (12)$$

$$x_2^e = \frac{c_2}{c_1} u_2^0 \frac{1+kz^2}{1+k^2 z^2} \quad (13)$$

where the diemensionless variable $z = (x_4^e / u_2^0)$. It is clear that from (10) and (11) one can get

$$x_3^e = 0 \quad (14)$$

$$c_5 (x_2^e z - x_1^e) u_2^0 = T_L + \frac{c_3}{c_4} \omega_{ref} \quad (15)$$

From the definition of z and collecting (12)-(14), the equilibrium point can be deduced as

$$\begin{bmatrix} x_1^e \\ x_2^e \\ x_3^e \\ x_4^e \end{bmatrix} = \begin{bmatrix} \frac{c_2}{c_1} \frac{1-k}{1+k^2 z^2} u_2^0 z \\ \frac{c_2}{c_1} \frac{1+kz^2}{1+k^2 z^2} u_2^0 \\ 0 \\ u_2^0 z \end{bmatrix}. \quad (16)$$

Which gives a nonunique equilibrium point, which is dependent on a dimensionless variable z. It satisfies the following polynomial equation

$$kz^3 - z^* k^2 z^2 + kz - z^* = 0. \quad (17)$$

This a third-order polynomial with dimensionless coefficients depend on the tunning gain k and load torque denoted as
$z^* = \left[(T_L + \frac{c_3}{c_4} \omega_{ref}) c_1 / c_5 c_2 (u_2^0)^2 \right]$. The real roots of (17) give equilibrium points values for any given gain k and any given load z^*. It is noticed that (17) has at least one and at

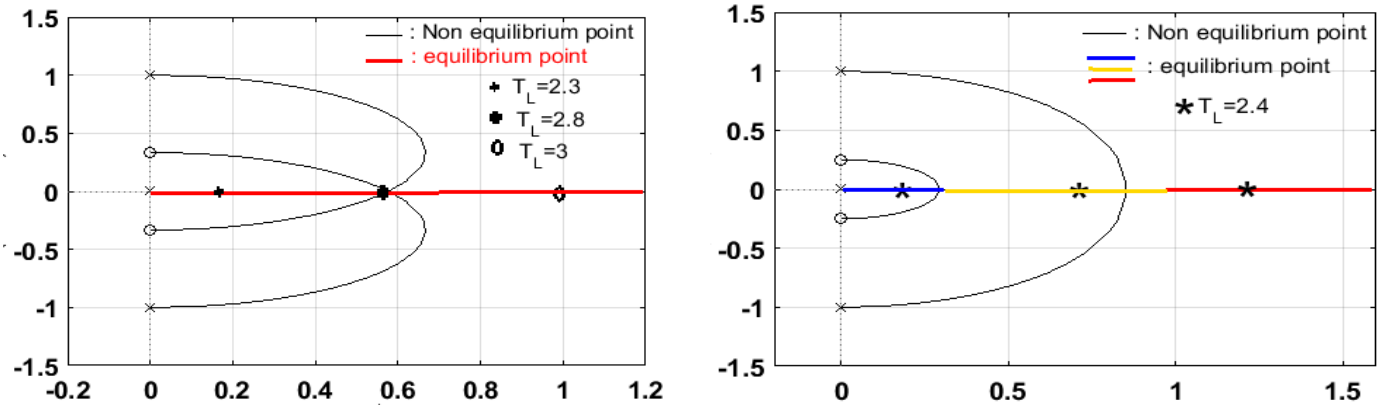

Fig. 2. Locus of the system equilibria as a function of load torque T_L. (a) k = 3 and (b) k = 4.

most three real solutions. The roots can be obtained by using of root locus method for the appropriate form of (17) as

$$1 - z^* \frac{(k^2z^2+1)}{kz^3+kz} = 0. \qquad (18)$$

Fig. (2a) proofs that the uniqueness of the equilibrium point for $k \leq 3$. It is clear that three corresponding real equilibria are there for the single value of z^*. For different other values of z^*, there is a singular real equilibrium point. It is evident from Fig. (2b), the nonuniqueness of equilibria for $k > 3$. Three distinct real equilibrium points for a definite range of z^*.

B. Local stability Analysis

The stability of the equilibrium point is investigated according to the eigenvalues of the characteristic equation

$$|\lambda \mathbf{I} - \mathbf{J}| = 0 \qquad (19)$$

where λ, **I,** and **J** are the eigenvalue, identity matrix, and the Jacobian matrix, respectively, of the system (4)-(7) evaluated at the equilibrium point $(x_1^e, x_2^e, x_3^e, x_4^e)$ which has the expression given by (20), as illustrated at the undermost of this page.

The model has been simulated for the value of parameters $c_1 = 13.67\ \mathrm{s}^{-1}$, $c_2 = 1.56\ \mathrm{Hs}^{-1}$, $c_3 = 0.59\ \mathrm{s}^{-1}$, $c_4 = 1176\ \mathrm{kg}^{-1}\mathrm{m}^{-2}$, $c_5 = 2.86$, $u_2^o = 4$ A, ω_{ref}181.1 rad/s. For different values of k, k_p, T_L and including $k_i = 0.2$, the solution of (19) will lead to fourth-order polynomial. Consequently, the equilibrium point $(x_1^e, x_2^e, x_3^e, x_4^e)$ has four possible roots; two pairs of complex conjugate roots, or two real roots plus pair of complex conjugate roots, or four real roots. Numerical analysis can be achieved and is focussed on the influence of the varying the proportional controller gain k_p. The simulation results are observed for different cases of load torque as listed in Table 2. The dynamics undergo qualitative changes due to the variations of parameter k_p. When load torque $T_L = 2.3$ Nm and $k_p = 0.002$, a stable limit cycle is observed. However, for $k_p = 0.008$, the limit cycle disappears and the stable equilibrium point occurs.

$$J(k,z) = \begin{bmatrix} -c_1 & -kc_1z & 0 & c_2\frac{(1-k)}{1+k^2z^2} \\ kc_1z & -c_1 & 0 & kc_2\frac{(1-k)}{1+k^2z^2}z \\ c_4c_5u_2^0 & -c_4c_5u_2^0z & -c_3 & -c_4c_5\frac{c_2}{c_1}u_2^0\frac{(1+kz^2)}{1+k^2z^2} \\ k_pc_4c_5u_2^0 & -k_pc_4c_5u_2^0z & k_i - k_pc_3 & -k_pc_4c_5\frac{c_2}{c_1}u_2^0\frac{(1+kz^2)}{1+k^2z} \end{bmatrix} \qquad (20)$$

Table 2 Eigenvalues corresponding for k_p, T_L, and k.

	T_L	Equilibrium point	k_p			
			0.002		0.008	
			Eigenvalues	Type of attractor	Eigenvalues	Type of attractor
$k=3$	2.3	$(-0.13,0.37,0,0.8)$	$0.247+20.93i, 0.247-20.93i, -19.51, -11.44$	Limit cycle	$-5.56+22.42i, -5.56-22.42i$ $-13.46+1.54i, -13.46-1.54i$	Spiral node
	2.8	$(-0.13,0.23,0,2.28)$	$-11.81+25.86i, -11.81-25.86i$ $-5.83, -0.006$	Spiral node	-14.51+26.77i, -14.51 -26.77i -5.07 , -0.006	Spiral node
	3	$(-0.09,0.18,0,4)$	$-13.94+41.94i, -13.94-41.94i$ $-0.63+5.9i, -0.63-5.9i$	Spiral node	$-15.28+41.67i, -15.28-41.67i$ $-1.13+5.8i, -1.13-5.8i$	Spiral node
$k=4$	2.4	$(-0.07,0.13,0,4.5)$	$-14.07+62.01i, -14.07-62.01i$ $-0.33+5.21i, -0.33-5.21i$	Spiral node	$-14.97+61.59i, -14.97-61.59i$ $-0.74+5.2i, -0.74-5.2i$	Spiral node
		$(-0.11,0.16,0,2.48)$	$-13.39+35.81i, -13.39-35.81i$ $-7.19, 4.97$	Spiral focus	$-15.56+36.08i, -15.56-36.08i$ $-6.4208, 5.2710$	Spiral focus
		$(-0.15,0.34,0,0.68)$	$0.45+22.13i, 0.45-22.13i$ $-22, -9.15$	Limit cycle	$-5.72+24.43i, -5.72-24.43i$ $-9.76, -16.06$	Spiral node

It is evident that the complex eigenvalue crosses the imaginary axis and causes a Hopf bifurcation occurs.

C. Bifurcations

In this subsection, characterization of various dynamical behaviors obtained concerning the system parameters; k, T_L, k_p, k_i, is reported. The various bifurcation behaviors which can be obtained from IFOC current-driven induction motor. System (4)-(7) is solved numerically using the 4th order Rung-Kutta method. The time step is always $\Delta t = 0.002\ sec.$ for each set of parameters used in this paper. The system model is integrated for a long time. The bifurcation diagram is used to define the scenario type giving rise to complex dynamics. Also, the dynamics of the system can be identified using its spectrum of Lyapunov exponents. For fixed points, $L_{ex4} < L_{ex3} < L_{ex2} < L_{ex1} < 0$, for periodic orbits, $L_{ex1} = 0, L_{ex4} < L_{ex3} < L_{ex2} < 0$, for quasiperiodic orbits $L_{ex1} = L_{ex2} = 0, L_{ex4} < L_{ex3} < 0$, and for chaotic dynamics, $L_{ex1} > 0, L_{ex2} = 0, L_{ex4} < L_{ex3} < 0$.

The main bifurcation parameter k_p is considered, the system parameters are keeping at the values as defined in the previous subsection.

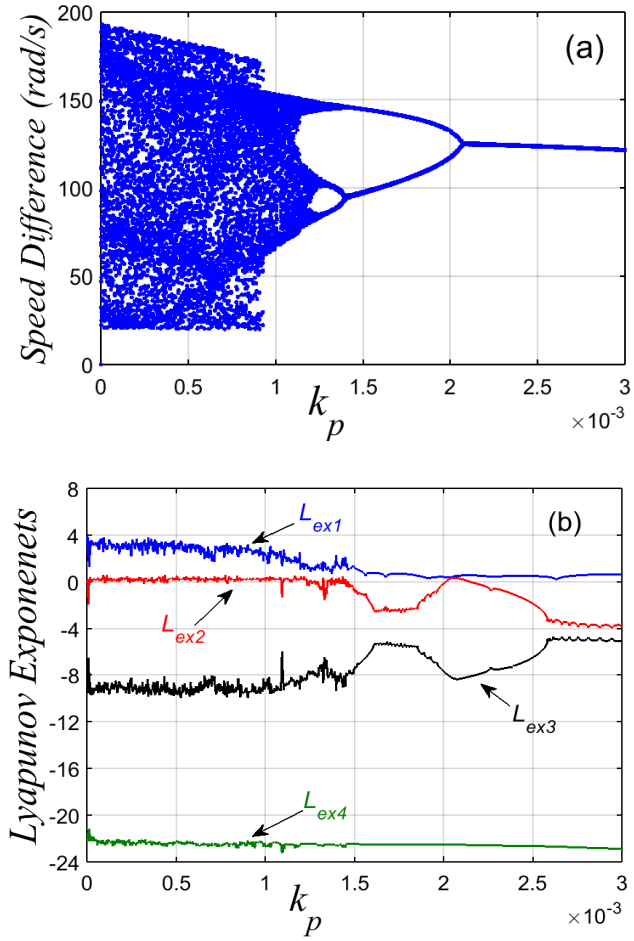

Fig.3(a) Bifurcation diagram and (b) corresponding Lyapunov exponents spectrum versus k_p.

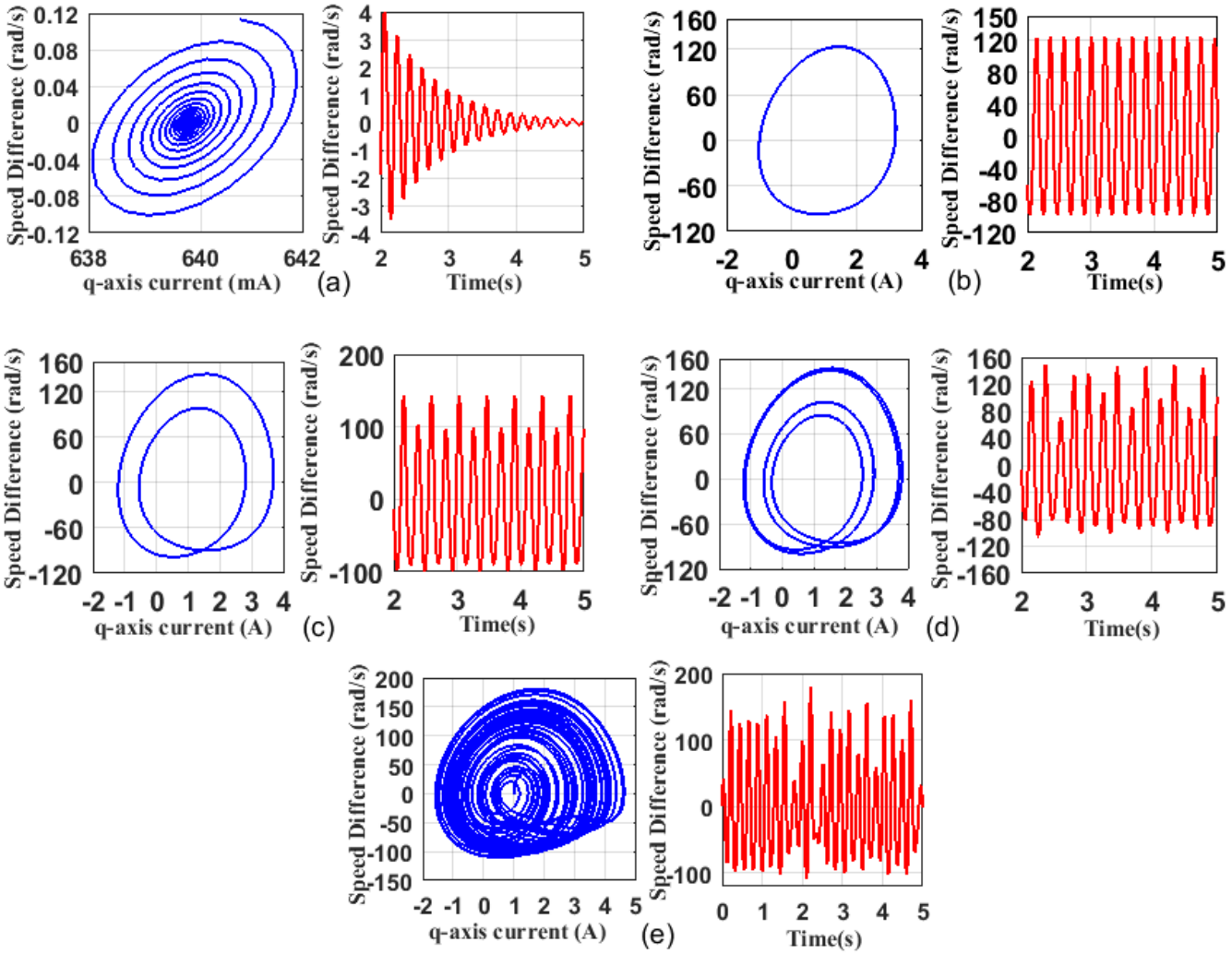

Fig.4 Phase portraite projected on (current, speed difference) plane (left column) and speed difference time response (right column): (a) stable equilibruim point for $k_p = 0.008$, ,(b) period-1; $k_p = 0.0025$, (c) period-2; $k_p = 0.00156$, (d) period-4; $k_p = 0.00129$, (e) chaotic attractor; $k_p = 0.0005$.

In the case of load torque value $T_L = 2$ Nm, $k_i = 0.55$, and $k = 3$, the bifurcation diagram and corresponding Lyapunov exponents spectrum for varying k_p are depicted in Figs. 3a and 3b, respectively. The bifurcation diagram is observed by capturing and plotting the maximum points of the speed difference in as a function of the parameter k_p in the range of $0 < k_p \leq 0.003$. According to Figs. 3a and 3b, when the bifurcation parameter k_p is heavily increased, the following bifurcation sequence emerges. For $k_p \geq 0$, the system displays chaotic dynamics. Further increasing the bifurcation parameter k_p beyond the critical valu $k_{pcr1} \approx 10^{-3}$, a period-8 oscillation appears.

When increasing up to $k_{pcr1} \approx 1.2 * 10^{-3}$, period-4 becomes clear. Thus, a period-doubling sequence leading to a quasi-periodic oscillation. It is clear that the bifurcation diagram and Lyapunov exponents spectrum are well agreed. Different numerical phase portraits on the $i_{qs} - (\omega_{ref} - \omega_r)$ plane and corresponding speed difference time domain waveform that observed are justifying the bifurcation sequences as illustrated in Fig.4. Which shows clearly that the speed difference goes to chaos through the route of period-doubling bifurcation with the parameter gain k_p decreasing gradually. As can be seen from Fig. 4a, the trajectory settles into a stable

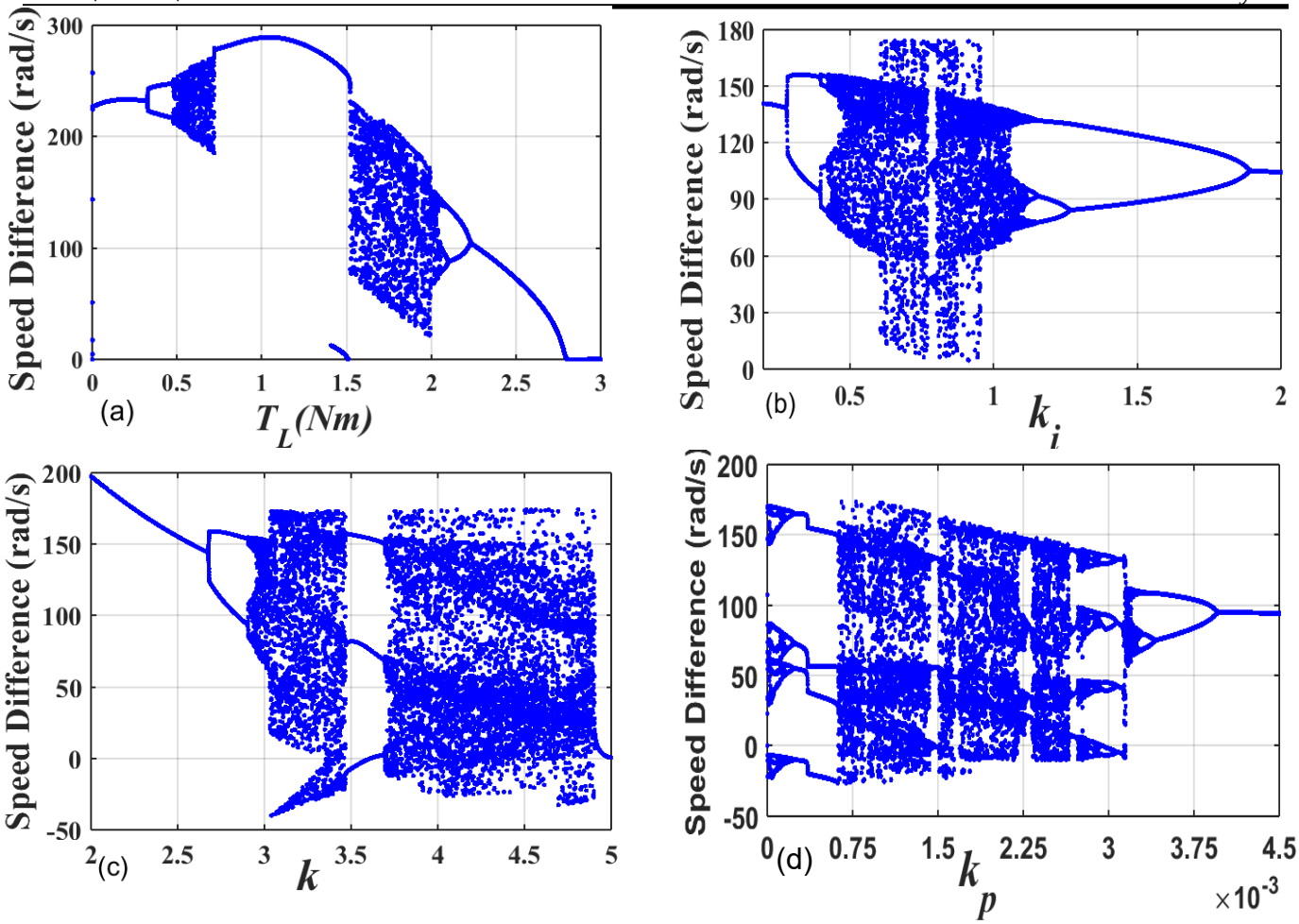

Fig. 5. Bifurcation diagrams showing local maxima of the coordinate speed difference $(\omega_{ref} - \omega_r)$ of the attractor obtained for varying, respectively, T_L, k_i , k and k_p: (a) T_L is a parameter and $k_i = 0.55$, $k = 3$, $k_p = 0.001$, (b) k_i is a parameter and $T_L = 2\ Nm$, $k = 3$, $k_p = 0.001$, (c) k is a parameter and $k_i = 0.55$, $T_L = 2$ Nm, $k_p = 0.001$, (d) k_p is a parameter and $k_i = 0.55$, $T_L = 2$ Nm, $k = 4$.

equilibrium point, but there exists long-time transient behavior.

Next, the verification of Hopf bifurcation. For the values of k_p below the critical value $k_{pHopf} \approx 0.006$, the IFOC induction motor exhibits limit cycle operation (i.e. oscillations). The corresponding behavior is depicted in Fig. 4b. It can be seen that $(\omega_{ref} - \omega_r)$ oscillates with a constant speed when $k_p = 0.0025$. Along with the decreasing bifurcation parameter k_p, the speed difference exhibits the stable period-2 orbits, as shown in Fig. 4c. The onset of the period-4 solution is predicted for $k_p = 0.00129$. This is shown in Fig. 4d. The collision between the period-4 limit cycle.

and unstable equilibrium point takes place for $k_p = 0.0005$, as shown in Fig.4e. This gives rise to the chaotic attractor.

The dynamics sensitivity of IFOC induction motor system concerning control parameters k_i, k_p, load torque T_L, and the ratio k, analyzed through the bifurcation diagrams as shown in Fig.5. It highlights the symmetry, periodic windows, and period-doubling bifurcations. According to the bifurcation diagram of Fig.5b, a certain range of multiple attractors can be specified for k_i near 0.76. For the values of k_i in this domain, the behavior of the system dynamics extremely influences in the initial conditions of states.

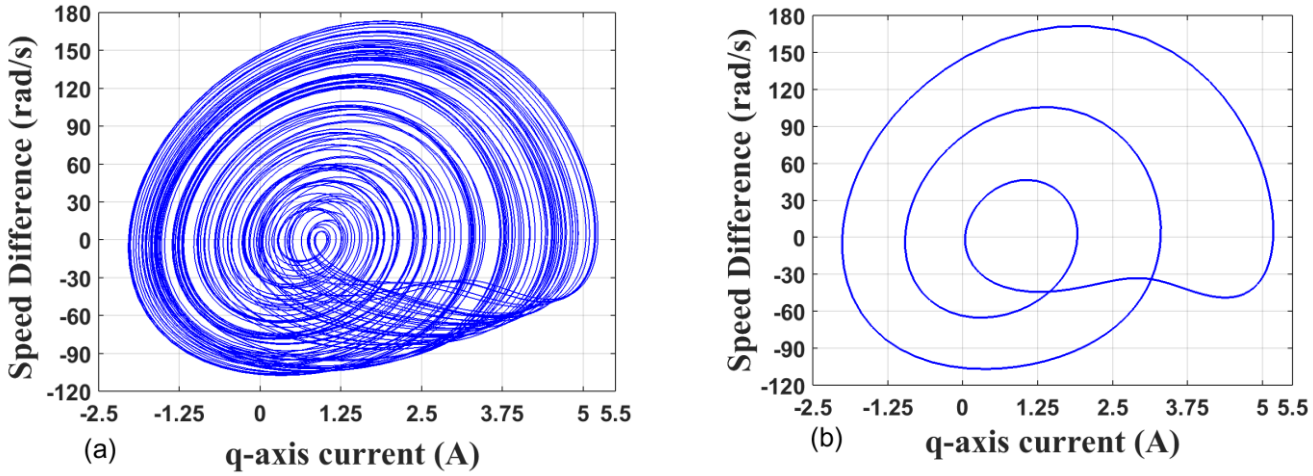

Fig. 6. Coexistence of multiple attarctors; chaotic attractor with period-3 for $k_i = 0.764$. The initial states values $(x_1(0), x_2(0), x_3(0), x_4(0))$ are:(a) $(0, 0.4, 150, 1)$ for the chaotic attarctor and (b) $(0, 0.4099, 119.99, 1)$ for period-3 limit cycles. $k_p = 0.001$, $T_L = 2$ Nm, $k = 3$.

The system has notable phenomena of multiple coexisting attractors. Two different attractors can be obtained (see Fig.6) concerning different initial state values. For example, the chaotic attractor of Fig. 6a generated from the initial conditions $x_1(0) = 0$, $x_2(0) = 0.4$, $x_3(0) = 150$, and $x_4(0) = 1$; while Fig. 6b is obtained from the initial values $x_1(0) = 0$, $x_2(0) = 0.4099$, $x_3(0) = 119.99$, and $x_4(0) = 1$, a period-3 attractor is observed. It is important to confirm that, the phenomena of multiple stability involving the coexistence of two different attractors were not previously reported in an IFOC induction motor drive system. Therefore, it appears as a good contribution related to the dynamics of the induction motor drive system. Also, the appearance of coexistence multiple attractors is not desirable and solely the need for control.

VI. CONCLUSION

In this brief, the dynamical analysis of IFOC current fed induction motor system model has been achieved. The equilibrium uniqueness and non-uniqueness have been investigated according to the estimated rotor resistance ratio. The uniqueness of equilibrium points is ensured for the estimated rotor resistance ratio located in the range of 300%. For a high value of rotor resistance ratio, k, three equilibrium points are created. Two of the equilibrium points are asymptotically stable and the other one is unstable. The effect of PI controller gains parameters and load torque on the bifurcations has been addressed more specifically. The bifurcation analysis shows that the complex dynamics and nonlinear oscillations can be grown in the IFOC induction motor system following the period-doubling bifurcation. It is clear that the IFOC induction motor drive system suffers from the uncommon behavior of coexistence multiple attractors for a certain range of integral gain k_i of the PI controller.

REFERENCES

[1] S. Ramadhan, and F. Rahma, "Analog Programmable Circuit Implementation for Memristor", Iraqi Journal for Electrical & Electronic Engineering, Vol. 14, No. 1, 2018.

[2] M. Abdullah, F. Rahma, and K. Abdul-Hassan, "Sliding Mode Control-Based Chaos Stabilization in PM DC Motor Drive", Iraqi Journal for Electrical & Electronic Engineering, Vol. 12, No. 2, 2016.

[3] O. Hussain, and F. Rahma, "Adaptive Control-based synchronization of chaotic systems with uncertain parameters and its application", Basrah Journal for Engineering Science, Vol. 16, No. 1, 2016.

[4] F. Rahma, and L. Fortuna, "Chaos Control in The Smallest Transistor-Based Chaotic Circuit", Islamic College University Journal, Vol. 29, 2014.

[5] F. Rahma, G. Al-Suhail, and M. Abd, " String of scrolls from a time-delayed chaotic circuit", International Journal of Simulation and Process Modelling, Vol. 13, No. 5, 2018.

[6] B. Bose, Power Electronics and AC Drives, Englewood Cliffs, NJ, Prentice-Hall, 1986.

[7] M. Montanari, S. Peresada, C. Rossi, and A. Tilli, "Speed sensorless control of induction motors based on a reduced-order adaptive observer", IEEE Transactions on Control Systems Technology, Vol. 15, No. 6, 2007.

[8] H. Khalil, E. Strangas, and S. Jurkovic, "Speed observer and reduced nonlinear model for sensorless control of induction motors", IEEE Transactions on Control Systems Technology, Vol. 17, No. 2, 2008.

[9]D. Holmes, B. McGrath, and S. Parker, "Current regulation strategies for vector-controlled induction motor drives", IEEE Transactions on Industrial Electronics, Vol. 59, No. 10, 2012.

[10] P. Alkorta, O. Barambones, J. Cortajarena, and A. Zubizarrreta, "Efficient multivariable generalized predictive control for sensorless induction motor drives", IEEE Transactions on Industrial Electronics, Vol. 61, No. 9, 2013.

[11] R. Krishnan and F. Doran, " Study of parameter sensitivity in high-performance inverter-fed induction motor drive systems", IEEE Transactions on Industry Applications, Vol. IA-23, No. 4, 1987.

[12] S. Maiti, C. Chakraborty, Y. Hori, and M. Ta, "Model reference adaptive controller-based rotor resistance and speed estimation techniques for vector controlled induction motor drive utilizing reactive power", IEEE Transactions on Industrial Electronics, Vol. 55, No. 2, 2008.

[13] C. Verrelli, A. Savoia, M. Mengoni, R. Marino, P. Tomei, and L. Zarri, "On-line identification of winding resistances and load torque in induction machines", IEEE Transactions on Control Systems Technology, Vol. 22, No. 4, 2013.

[14] A. Bazanella, and R. Reginatto, "Robustness margins for indirect field-oriented control of induction motors", IEEE Transactions on Automatic Control, Vol. 45, No. 6, 2000.

[15] L. Yang, X. Ma, and D. Dai, "Hopf bifurcation in doubly fed induction generator under vector control", Chaos, Solitons & Fractals, Vol. 41, No. 5, 2009.

[16] A. Bazanella and R. Reginatto, "Robust tuning of the speed loop in indirect field oriented control of induction motors", Automatica, Vol. 37, No. 11, 2001.

[17] M. Duran, F. Salas, and M. Arahal, "Bifurcation analysis of five-phase induction motor drives with third harmonic injection", IEEE Transactions on Industrial Electronics, Vol. 55, No. 5, 2008.

[18] G. Chen, D. Hill, and X. Yu, Bifurcation Control: Theory and Applications, Springer Science & Business Media, Vol. 293, 2003.